Korean J. Chem. Eng., **21**(3), 726-732 (2004)

Experimental Investigation into Compression Properties of Integrated Coal Gasification Combined Cycle Fly Ashes on a Ceramic Filter

Joo-Hong Choi†, Young-Cheol Bak, Hyuk-Jin Jang, Jin-Hyung Kim and Jin-Hyun Kim

Department of Chemical Engineering and ERI, Gyeongsang National University, Jinju 660-701, Korea
(*Received 2 September 2003 • accepted 5 November 2003*)

Abstract−The compression properties of IGCC (integrated coal gasification combined cycle) fly ash cake on a ceramic filter were carefully investigated under well-controlled conditions. Overall cake porosity and pressure drop of dust cake of three different particles of geometric mean diameters of 3.7, 6.2, and 12.1 μm, and dynamic shape factors of 1.37, 1.57 and 1.65, respectively, were investigated, at face velocities of 0.02-0.06 m/s. Overall cake porosity was strongly dependent on face velocity, mass load, and particle size. The expressions for overall cake porosity, considering the compression effect, and pressure drop across the dust cake were developed with good agreement with experimental results.

Key words: Gas Filtration, Ceramic Filter, Dust Cake Compression, Cake Porosity, Pressure Drop

INTRODUCTION

Although the pressure drop is a primary factor for design and operation of a filtering system, it has been difficult to predict exactly the pressure drop. One of the main reasons for this is due to the complicated compression properties of dust cake depending on system, dust source, and operation condition. Several investigators [Aguar and Coury, 1996; Choi et al., 2002; Endo et al., 1998; Schmidt, 1995] reported that the dust cakes were compressed during the filtration. Aguir and Coury [1996] measured directly the local porosity of limestone cake on a fiber filter by image analysis of the cake cross sections and showed that local cake porosity decreased in the direction to the filter from the cake surface. Höflinger et al. [1994] applied the Mohr-Coulomb deformation criteria to explain the cake compression, for spherical particles, based on the maximum inter-particle adhesion force and the friction angle between particles. According to this model, cake thickness reduction occurs when particles move due to the exceeding shear force developed by the lately formed dust layers. Neiva et al. [1999] proposed a cake buildup model in which the compression of a given dust layer was related with the drag forces of its upper layers. The computer programs [Höflinger et al., 1994; Neiva et al., 1999; Schmidt, 1995, 1997] for calculating pressure drop across dust cake (ΔP_c), based on the theories mentioned above, have shown good agreement with experimental results. However, they are valid in a limiting case and workable with specific parameters depending on every specific case. The dust cake compression depends on many co-dependent factors from the particle properties (shape, size, and density) [Choi et al., 2002a, b; Schulz, 1994], the filter surface [Herry, 1973], the gas properties (density, viscosity and humidity) [Gupta et al., 1993], and the operation conditions (face velocity and cleaning method) [Dennis and Dirgo, 1981; Silva et al., 1999].

The most interesting point is how to obtain a general and explicit equation for ΔP_c considering the compression effect. A semi-empirical equation derived by Kozeny & Carman is based on the assumption that dust cake is composed of a series of parallel capillaries. It is less applicable for polydisperse particles because uniform pore size is assumed in the model. The results calculated by this model show high deviation with experimental data for a dust cake of fine particles having a cake porosity greater than 0.7-0.8 [Perry, 1973]. A theoretical equation derived by Rudnick and First is based on Happel's cell model [Chung and Tsai, 1998]. It treats dust cake as an assemblage of individual particles. Each cell contains a particle surrounded by an imaginary concentric spherical shell. Here the porosity of the dust cake is equal to the ratio of the volume difference between the spherical shell and the particle to that of the spherical shell. This equation is applicable to polydisperse particles using the geometric mean diameter and the particle size distribution, but is not suitable to explain the dust compression effect. Endo et al. [1998] derived a more general equation considering the dynamic shape factor of particles and the particle size distribution. However, it is also restricted due to the assumption of uniform porosity through the overall cake. Moreover, they did not offer an exact value for the void function involved in the equation for denoting the compression effect.

There are very few reports of careful studies to investigate the compression properties of the cake because it is very difficult to measure the cake porosity under experimental conditions. In addition, the pressure drop across IGCC fly ash cake shows a very different pattern from that of conventional power plants or incinerators because the particles are composed of agglomerates of very fine carbon particles (mostly of nanometer size) [Choi et al., 2002c; Iwadate et al., 1998]. The aim of this study was to investigate the compression properties of IGCC dust cake under well-characterized conditions to propose an experimental equation for the pressure drop involving the compression effect.

EXPERIMENTAL

Fig. 1 is the schematic diagram of the experimental unit. The constant volume of IGCC fly ash was fed in the air stream with a screw feeder at room temperature. Two cyclones of different collection efficiencies using a different dimension (diameters of conventional

†To whom correspondence should be addressed.
E-mail: jhchoi@nongae.gsnu.ac.kr

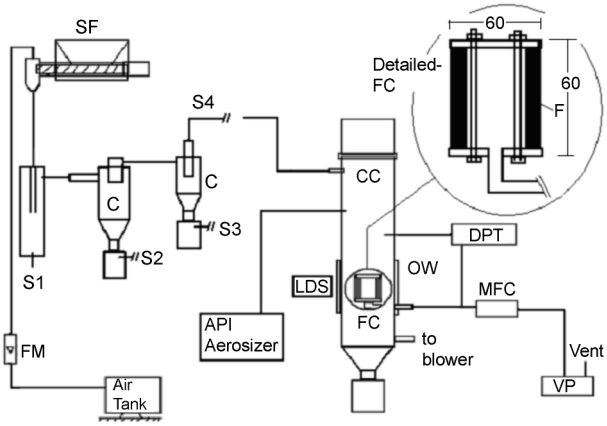

Fig. 1. Experimental unit for measuring the filtration properties of fly ashes.
Cyclone (C), Cell Chamber (CC), Differential pressure transmitter (DPT), Dust stream (S), Filter (F), Filter cell (FC), Flow meter (FM), Laser displacement sensor (LDS), Mass flow controller (MFC), Optical window (OW), Screw feeder (SF), Vacuum pump (VP)

type are 64 and 48 mm for 1st and 2nd one, respectively) were used sequentially to obtain dust streams of different particle sizes. Consequently, the mean diameter of particles in dust stream decreases in the order of S2>S3>S4, where S2 and S3 are dust streams chosen from bottom flows of the first and the second cyclone, respectively, and S4 is the outlet stream of the second cyclone. The large particles being settled naturally in the flow were previously removed in a settling chamber (S1). By this method, well-distributed particle streams (S2, S3, and S4) were successfully obtained. In order to carry out an experiment for certain particle sizes, part of one particle stream was connected to pass the cell chamber by suction with a blower. Part of this dust stream was forced to cross the filter from outside to inside by sucking with a vacuum pump while the excess stream passed out the cell chamber. By this method, particles accumulated on the outside filter surface. Face velocity across the filter was constantly controlled with a mass flow controller even though pressure drop changed during the run time. Pressure drop across the filter was measured with a differential pressure transmitter connected to the cell chamber and the outlet of the filter unit. Pressure drop versus time (ΔP-t) curve at a constant face velocity was recorded while the cake thickness was measured with a laser displacement sensor (Model LK-081/2011/C2, Keyence Corp., Osaka, Japan) under experimental conditions. The sensor was located at the outside of the cell chamber. And its light passed through an optical window. The measuring insight spot of the optical window was continuously cleaned by air-jet injection to remove dust deposition. The sensor measures the distance between the sensor and the cake surface on a fixed position. Part of the dust stream from the cell chamber was accepted

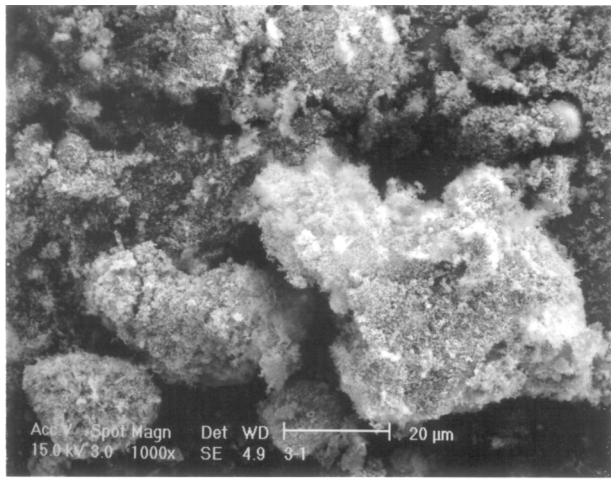

(a)

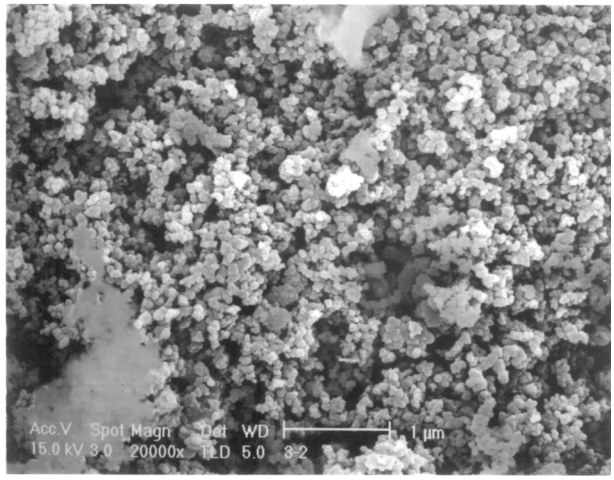

(b)

Fig. 2. SEM images of typical IGCC fly ash: 1,000× (a) and 20,000× (b).

to be introduced into an aerodynamic particle size analyzer (API Aerosizer, manufactured by Amherst Process Instruments, Inc., Amherst, MA) to measure the particle size distribution under experimental conditions.

Cylindrical SiC filter (Dia-Shumalith 10-20, manufactured by Schumacher Umweltund Trenntechnik, Germany) [Shulz and Durst, 1998] of dimensions of 60 mm and 10 mm (outer diameter and thickness), respectively, was used in the study. The filter of 50 mm length was assembled between two flanges and formed filter cell in the cell chamber as shown in Fig. 1. The filter has a thin outer membrane layer whose mean pore size is about 10 μm and has a collection efficiency of more than 99.999% for 0.5 μm particle [Hemmer et al., 1999]. Mass load (W) of accumulated-particulates on the filter

Table 1. Properties of particles in the dust streams

Dusty dust stream	ρ_p (g/cm^3)	d_g (μm)	d_v (μm)	d_s (μm)	σ_g (μm)	κ	Carbon (wt%)
S2 (1st cyclone bottom)	2.27	12.1	13.3	10.4	1.6	1.65	38.1
S3 (2nd cyclone bottom)	2.25	6.2	7.3	5.8	1.6	1.57	45.9
S4 (2nd cyclone top)	2.20	3.7	4.8	4.1	1.5	1.37	47.3

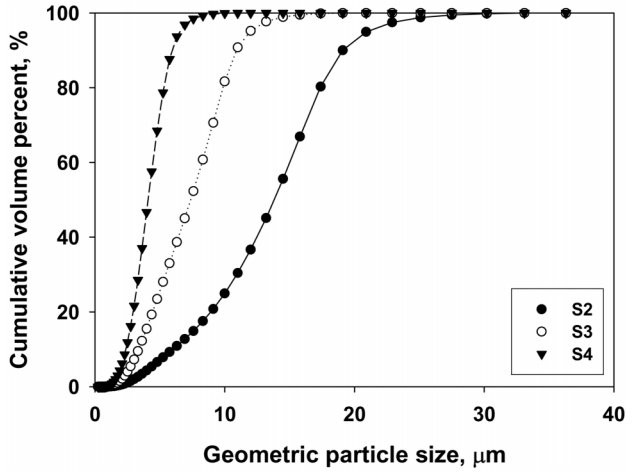

Fig. 3. Particle size distribution of classified particle streams.

surface was calculated by measurement of the weight difference of the filter before and after the run with an electrical balance. It was tested that mass load increased linearly with a run time (normally less than 30 minutes) for a constant feeding rate of the particulates.

Fly ash used in this study was from the process development unit (PDU) for IGCC located at the Institute for Advance Engineering (IAE), and collected in the filtering unit by using SiC filters (Dia-Shumalith 10-20) at a temperature of 573-673 K. The fly ash in classified-particle streams contains the unburned-carbon (C) more than 38 wt.% as shown in Table 1. The particles are composed of agglomerates with 100-200 nm particles as shown SEM images of Fig. 2.

RESULTS AND DISCUSSION

1. Particle Properties in the Dust Streams

Fig. 3 shows the cumulative volume percent of the geometric diameter of particles, in each stream, measured by API Aerosizer. The results imply that it is successful in obtaining particle streams of different sizes by series operation of two cyclones even though parts of particles in the border ranges are overlapped. The statistical analysis of the measurement data tells us the geometric mean diameter (d_g), the volumetric mean diameter (d_v), and the geometric standard deviation (σ_g), which are shown in Table 1. The dynamic shape factor (κ) of a particle is defined as its drag force at a given velocity divided by the drag force at the same velocity of a sphere of the same volume as the particle [Davies, 1979]. It is expressed by Eq. (1), where, d_e is the equivalent spherical diameter of the particle having the same volume with the particle, d_s is Stokes diameter corresponding to the terminal velocity in a viscous flow, C_e and C_s are Cunningham correction factors of particles corresponding to diameters d_e and d_s, respectively, at the velocity. Cunningham correction factors are 1.16 and 1.0 for the particles of 1 and 10 μm, respectively, at normal state (1 bar and room temperature). It decreases as particle diameter increases. The Cunningham correction factor (C) of particles larger than 0.1 μm is expressed by Eq. (2) [Hinds, 1999], where λ is mean free path of the fluid. The mean free path of air is 0.066 μm at normal state. d_e is projected area diameter which is equivalent to a circle diameter having the same area of the particle [Hemmer et al., 1999]. However, there are many arguments about what does represent the equivalent diameter exactly for polydisperse particles. The volumetric mean diameter (d_v) measured by API Aerosizer was used as the equivalent diameter in this study. The Stokes diameter is also replaced with the Stokes mean diameter (d_s) for the polydispersed particles. Finally, dynamic shape factor was calculated by Eq. (3).

$$\kappa = \frac{C_e}{C_s}\left(\frac{d_e}{d_s}\right)^2 \tag{1}$$

$$C = 1 + \frac{2.52\lambda}{d} \tag{2}$$

$$\kappa = \frac{C_v}{C_s}\left(\frac{d_v}{d_s}\right)^2 \tag{3}$$

The Stokes diameter was obtained by the sedimentation method [Webb and Orr, 1997]. In this method, the particles are suspended in water in a glass tube of 12 mm inner diameter. The concentration change of the solid suspended with time is determined by measuring the light absorbance at wavelength 320 nm. The Stokes mean diameter d_s is obtained at the point where the cumulative mass fraction reaches 0.5. Table 1 shows the dynamic shape factors of the classified-particle are 1.37-1.65 μm depending on the size.

The composition of unburned carbon (C%) was determined by measuring the weight change of the sample by thermal gravimetric analyzer (TGA). The sample was heated at the rate of 30 K/min from room temperature to 1,223 K and finally kept for 60 minutes at that temperature. It was assumed that carbon was burned naturally in the analysis cell above a certain temperature. Carbon contents were assumed to be equivalent to the weight changes corresponding to temperature above 873 K (after 20 minutes from the start) and were summarized in Table 1. Carbon content increased as the particle size decreased. Particle density (ρ_p) in Table 1 was obtained with a Le Chatelier's density bottle by measuring the true volume of the particle for the given mass. Density of the particle decreased as particle size decreased because carbon content increased as mentioned above.

2. Cake Porosity Expression

The increasing rate of cake thickness (H) decreased gradually and then kept constant after a certain mass load. These results are typical patterns showing the compression phenomena of the cake, which can be assumed by the cake build up model proposed by Schmidt [1995]. In the model, dust cake layer is divided into many thin layers having a thickness corresponding to the time duration. At the initial stage of a short time, the first layer is formed on the filter surface. During the next short time interval, the second layer is formed over the first layer. The first layer is compressed by the drag force developed by pressure drop across the new layer and is shrunk. When the third layer is formed, the first layer is shrunk more than the second layer by the compression forces from the sum of the second and third layers. Consequently, the porosity and thickness of the previously formed layers are reduced with the increase of mass load. However, the increasing rate of H becomes constant after a certain mass load because under a certain thickness the cake layer reaches an incompressible state. In order to inspect the compression property of IGCC fly ash cake on the ceramic filter, the thickness change of the cake was observed during the increase of the mass load by using a clean filter for each run. Fig. 4 shows the variation of the

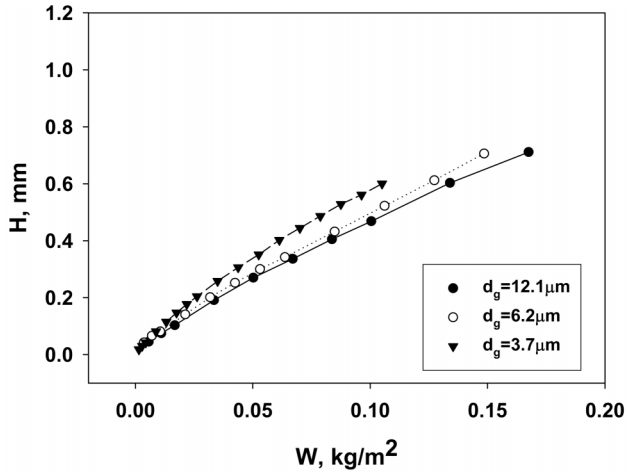

Fig. 4. Dependency of thickness change with mass load for the particle size variation for face velocity 0.06 m/s.

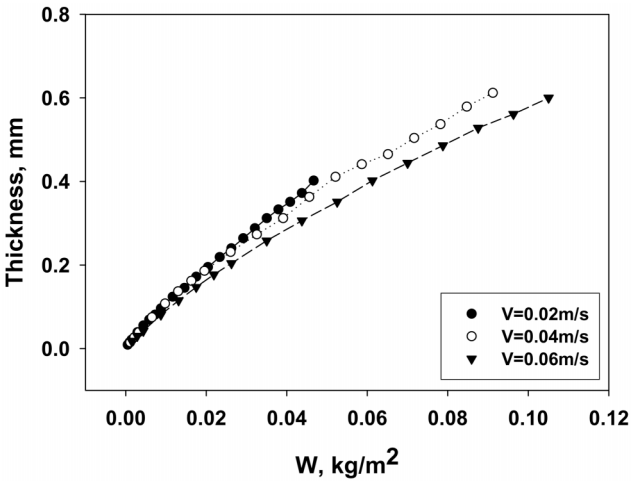

Fig. 5. Dependency of thickness change with mass load for the face velocity variation for particle size 3.7 μm.

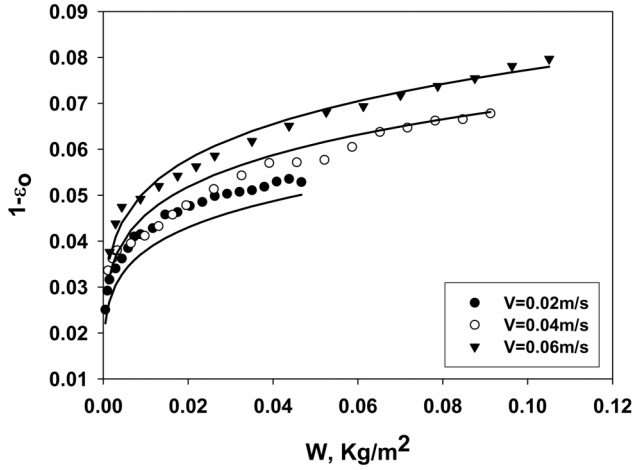

Fig. 6. Cake porosity dependency on W at various face velocity. Solid lines show the correlation curve to prepare the Eq. (6).

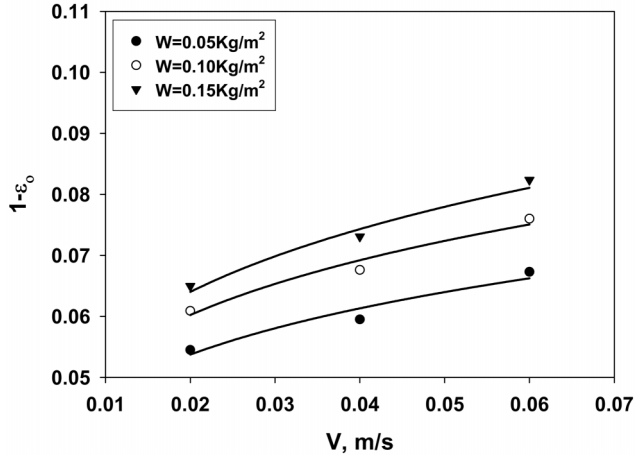

Fig. 7. Cake porosity dependency on v at various mass load. Solid lines show the correlation curve to prepare the Eq. (6).

thickness change according to the mass load for the gas streams of three different particle sizes at a face velocity 0.06 m/s. And Fig. 5 shows the variation of the thickness change according to the mass load for gas streams of particle size 3.7 μm at different face velocities described in the figure. Fig. 4 and Fig. 5 show that the increasing rate of H with W decreases gradually and keeps constant after a certain value of W. These experimental results represent the cake compression effects as described above by the cake build up model.

Fig. 4 also shows that small particles present higher thickness than the large ones for a given mass load in the same condition. This result is because the small particles form a cake of high porosity. Fig. 5 shows that the cake thickness decreases as the face velocity increases. This is because that face velocity predominantly affects pressure drop which acts as the main drag force on cake deformation. Pressure drop across a rigid porous layer increases linearly with face velocity [Neiva, 1999]. According to the results shown in Fig. 4 and Fig. 5, the cake porosity predominantly depends on face velocity, mass load, and particle size.

Overall cake porosity ε_o was calculated by Eq. (4) [Cheung and Tsai, 1998]. It denotes the average value across the entire dust layers. The experimental result shows that ε_o decreases exponentially with H.

$$\varepsilon_o = 1 - \frac{W}{\rho_p H} \tag{4}$$

The general trends of overall cake porosity change with the variation of W, v, and d_g are plotted in Fig. 6 and Fig. 7 for the case of S4 (dg=3.7 μm) depending on mass load and face velocity, respectively. The experimental values of $1-\varepsilon_o$ were closely correlated with the equation of the power order on mass load (Fig. 6) and face velocity (Fig. 7). Table 2 and Table 3 represent the corresponding power order constants b and d for the variation of W and v, respectively, for all cases of experimental data. The average values 0.18 (standard deviation 0.017) and 0.27 (standard deviation 0.055) for b and d, respectively, were used to prepare a general equation, representing all the experimental results for the overall cake porosity, such as Eq. (5). Solid lines in Fig. 6 and Fig. 7 represent the calculation values by Eq. (6). Correction efficient K in Eq. (5) was obtained

Table 2. The correlation constants to express overall cake porosity changes by $1-\varepsilon_o=aW^b$

d_g / v	12.1		6.2		3.7	
	a	b	a	b	a	b
0.02	0.10	0.15	0.09	0.17	0.09	0.16
0.04	0.12	0.19	0.11	0.17	0.10	0.18
0.06	0.14	0.17	0.15	0.21	0.11	0.18

Table 3. The correlation constants to express overall cake porosity changes by $1-\varepsilon_o=cv^d$

d_g / W	12.1		6.2		3.7	
	c	d	c	d	c	d
0.05	0.18	0.29	0.17	0.29	0.11	0.19
0.10	0.21	0.30	0.21	0.32	0.13	0.20
0.15	0.23	0.31	0.25	0.34	0.15	0.22

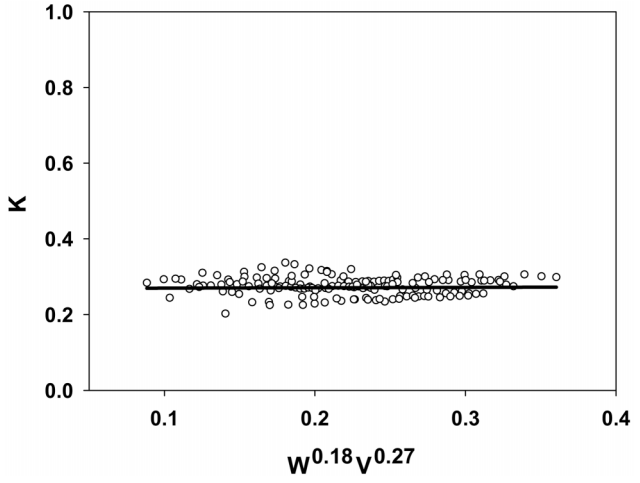

Fig. 8. The correlation plot of experimental data to obtain K in Eq. (5).

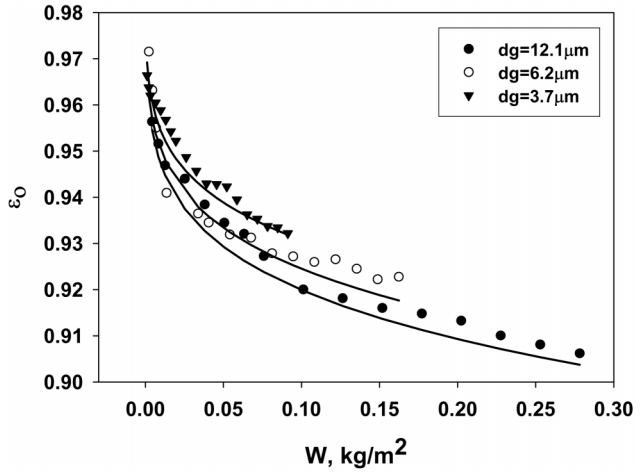

Fig. 9. The overall cake porosity change with W depending on particle size. Solid lines denote the values calculated with Eq. (6).

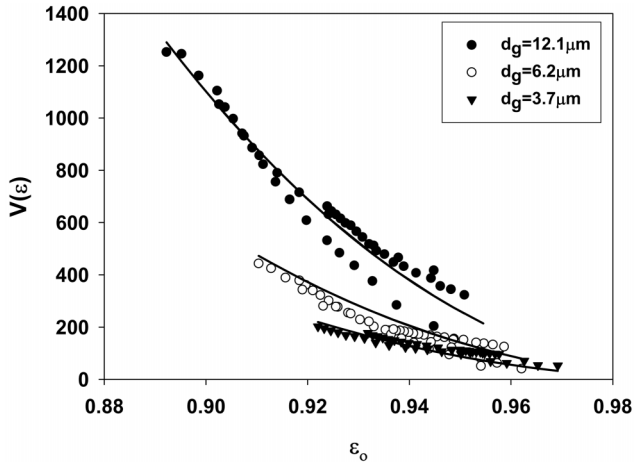

Fig. 10. The correlation plot for V(ε) at the variation of cake porosity and particle size. Solid lines denote the values calculated with Eq. (8).

through a correlation of the many experimental data for various particle sizes as shown in Fig. 8. The correlation of experimental data roughly produced the general constant 0.27 for the calculation of overall cake porosity changing in W and v. Eq. (6) presents the complete experimental equation for ε_o showing the effect of W, v, and d_g. Fig. 9 is the typical plot showing that the experimental data are closely expressed by Eq. (6) for the face velocity of 0.04 m/s.

$$1-\varepsilon_o = K v^{0.27} W^{0.18} \tag{5}$$

$$\varepsilon_o = 1-0.27 d_g^{0.15} v^{0.27} W^{0.18} \tag{6}$$

3. The Expression of Pressure Drop Across the Cake

The pressure drop across the cake (ΔP_c) is calculated with the difference between that across the total and the filter. Generally, ΔP_c increased sharply at the initial stage and then gradually increased showing the upward curvature according to mass load. However, previous workers [Cheung and Tsai, 1998; Neiva et al., 1999; Perry, 1973] tried to fit the experimental results with the linear equations depending on W and v for the conditioned filter. When considering particle shape, particle size deviation, and compressible property of the cake, Eq. (7) proposed by Endo et al. [1998] is the most suitable equation. Where μ is gas viscosity and $\nu(\varepsilon)$ is void function.

$$\Delta P_c = \frac{18\mu\kappa\nu(\varepsilon)}{\varepsilon^2}\cdot[\rho_p d_g^2 \exp(4\ln^2\sigma_g)]^{-1} v W \tag{7}$$

This equation adopts the uniform cake porosity and the linear dependency of ΔP_c on W and v. Many cases of experimental results carried out with a variation of particle size, face velocity, and mass load indicated that the experimental data of ΔP_c could be correlated by a power order equation on the variation of v and W with a power constant of more than 1.0. Now, the task is how to prepare a suitable equation involving the compression effect. In this study, we tried to find the proper expression for $\nu(\varepsilon)$ implying the compression effect on the cake porosity calculation by using the linear dependence on W and v to apply Eq. (7). Many sets $\nu(\varepsilon)$ and ε_o calculated from the experimental data of ΔP_c obtained under different conditions of particle size, the face velocity, and mass load are plotted in

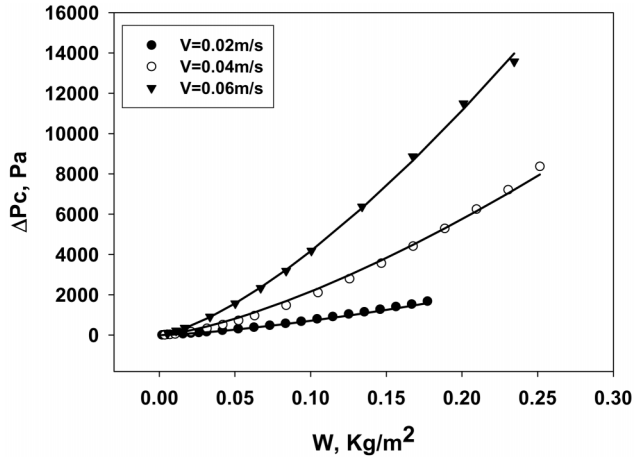

Fig. 11. The pressure drop change with W depending on v for 12.71 μm particles. Solid lines denote the values calculated with Eq. (9).

Fig. 10, where overall cake porosity (ε_o) was determined by Eq. (6). The correlation plot of the experimental data produced Eq. (8) to correlate the experimental values of $v(\varepsilon)$. This is a similar form of the equation, $10(1-\varepsilon)/\varepsilon$, which is the Kozeny-Carman expression that is valid for non-compressible, monodispersed, and relatively coarse particles. The value and the change of $v(\varepsilon)$ are much higher than that predicted by the Kozeny-Carman expression. This is because IGCC fly ash is more compressible by being composed of agglomerates based on very fine particles of nanometer size.

The overall pressure drop of dust cake was finally expressed by Eq. (9) for IGCC fly ash at room temperature. Fig. 11 shows that Eq. (9) successfully meets with the experimental data of ΔP_c for the particles streams of S2 (d_g is 12.1 μm). The correlation confidence of Eq. (9) is presented in Fig. 12, for the case of S4 (d_g is 3.7 μm), which shows the calculated values closely agree with the experimental data of ΔP_c. This modified-Endo equation is very useful to denote all the complicated effects from the particle properties (the particle size, the particle size distribution, and the dynamic shape factor), the operation conditions (face velocity and the mass load), and compression effect. However, it still has a restriction on the view

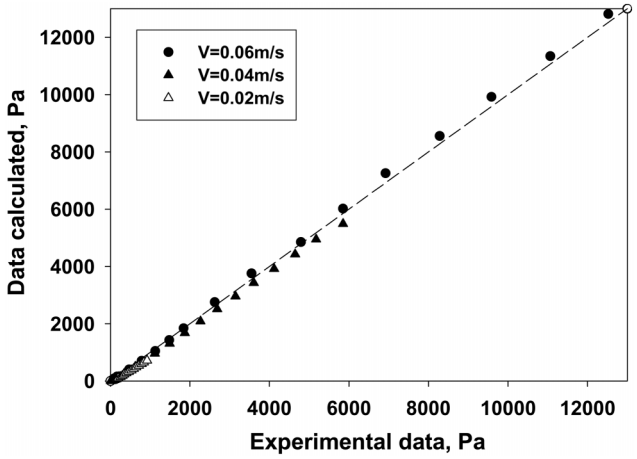

Fig. 12. Comparable plot of pressure drops of experimental data and calculated one by Eq. (9) for S3 (3.7 μm) particles.

of that it is applicable only on IGCC fly ash at room temperature. For particles of different type, alternative equations for v_o and $v(\varepsilon_o)$ should be obtained.

$$V(\varepsilon) = 10^{10} d_g^{0.92} \frac{(1-\varepsilon_o)^2}{\varepsilon_o} \tag{8}$$

$$\Delta P_c = \frac{18\times 10^{10} \mu\kappa (1-\varepsilon_o)^2}{\varepsilon_o^3} \cdot [\rho_P d_g^{1.08} \exp(4\ln^2\sigma_g)]^{-1} vW \tag{9}$$

CONCLUSIONS

Compression properties of IGCC fly ash cake on a ceramic filter were carefully investigated by cautious measurement of the cake thickness and pressure drop under experimental conditions. From the experimental data obtained by the change of the particle size, the face velocity, and the mass load, the following is concluded.

The experimental data for overall cake porosities were well correlated with mean particle size, mass load, and face velocity by the equation $\varepsilon_o = 1 - 0.27 d_g^{0.15} v^{0.27} W^{0.18}$, denoting the compression effect of the dust cake. The correlation of many cases of experimental results with the variations of the particle size, the face velocity, and mass load produced a general equation for the void function $V(\varepsilon) = 10^{10} d_g^{0.92} [(1-\varepsilon_o)^2/\varepsilon_o]$ which is involved in the equation proposed by Endo et al. [1998]. The modified-Endo equation applying the void function obtained in this study expressed well the experimental results for IGCC fly ash.

NOMENCLATURE

a, b, c, d : constants for empirical equations
C : Cunningham correction factor, C_e for d_e, C_v for d_v, and C_s for d_s
d_e : equivalent spherical diameter of particle [m]
d_g : geometric mean diameter of particles [m]
d_p : projected area mean diameter of particles [m]
d_s : Stoke's mean diameter of particles [m]
d_v : volume average mean diameter of particles [m]
H : mass cake thickness [m]
K : correction efficient
v : face velocity [$m \cdot s^{-1}$]
W : dust load based on the filter surface area [$kg \cdot m^{-2}$]
ΔP_c : pressure drop across dust cake [Pa]
ε_o : overall porosity of the entire cake layer [-]
κ : dynamic shape factor [-]
λ : mean free path of fluid [m]
μ : air viscosity [$kg \cdot s^{-1} \cdot m^{-1}$]
ρ_p : particle density [$kg \cdot m^{-3}$]
σ_g : geometric standard deviation [-]

ACKNOWLEDGMENTS

The authors would like to thank the Korea Energy Management Corporation, Korea Institute for Energy Research, and Institute for Advanced Engineering for their financial support.

REFERENCES

Aguar, M. L. and Coury, J. R., "Cake Formation in Fabric Filtration of

Gases," *Ind. Eng. Chem. Res*., **35**, 3673 (1996).
Cheung, Y. H. and Tsai, C. J., "Factors Affecting Pressure Drop Through a Dust Cake During Filtration," *Aerosol Science and Technology*, **29**, 315 (1998).
Choi, J. H., Ha, S. J. and Park, Y. O., "The Effect of Particle Shape on the Pressure Drop across the Dust Cake," *Korean J. Chem. Eng*., **19**, 711 (2002a).
Choi, J. H., Ha, S. J., Bak, Y. C. and Park, Y. O., "Particle Size Effect on the Filtration Drag of Fly Ash from a Coal Power Plant," *Korean J. Chem. Eng*., **19**, 1085 (2002b).
Choi, J. H., Ha, S. J. and Park, Y. O., "Pressure Drop Aspect of the Fly Ashes from Power Plants," 6th Intern. Aerosol Conference, Taipei, 1257 (2002c).
Davies, C. N., "Particle-Fluid Interaction," *J. Aerosol Sci*., **10**, 477 (1979).
Dennis, R. and Dirgo, J. A., "Comparison of Laboratory and Field Derived K_2 Values for Dust Collected on Fabric Filters," *Filtration and Separation*, **18**, 394 (1981).
Endo, Y., Chen, D.-R. and Pui, D. Y. H., "Effect of Particle Polydispersity and Shape Factor During Dust Cake Loading and Air Filters," *Powder Technology*, **98**, 241 (1998).
Gupta, A., Novick, V. J., Bisawas, P. and Monson, P. R., "Effect of Humidity and Particle Hygroscopicity on the Mass Loading Capacity of High Efficiency Particulate Air (HEPA) Filters," *Aerosol Science and Technology*, **19**, 94 (1993).
Hemmer, G., Berbner, S., Umhauer, H. and Kasper, G., "The Separation Efficiency of Ceramic Barrier Filters Determined at High Temperature by Optical Size and Concentration Measurement," High Temperature Gas Cleaning, Vol. 2, Ed. by A. Diller et al., 220 (1999).
Hinds, W. C., "Aerosol Technology," 2nd ed., Powells Books (1999).
Höflinger, W., Stöcklmyer, Ch. and Hackl, A., "Model Calculation of the Compression Behaviour of Dust Filter Cakes," *Filtration & Separation*, **December**, 807 (1994).
Neiva, A. C. B., Goldstein, Jr. L. and Calvo, P., "Modeling Cake Compressibility on Gas Filters," *High Temperature Gas Cleaning*, **2**, 83 (1999).
Perry, R. H. and Green, D. W., "Perry's Chemical Engineers' H/B," 6th ed., McGraw-Hill, 20 (1973).
Schmidt, E., "Experimental Investigations into the Compression of Dust Cakes Deposited on Filter Media," *Filtration & Separation*, **September**, 789 (1995).
Schmidt, E., "Theoretical Investigations into the Compression of Dust Cakes Deposited on Filter Media," *Filtration & Separation*, **May**, 365 (1997).
Schulz, K. and Durst, M., "Advantages of an Integrated System for Hot Gas Filtration Using Rigid Ceramic Elements," *Filtration & Separation*, **January/February**, 25 (1994).
Silva, C. R. N., Negrini, V. S., Aguiar, J. R. and Coury, M. L., "Influence of Gas Velocity on Cake Formation and Detachment," *Powder Technology*, **101**, 165 (1999).
Webb, P. A. and Orr, C., "Analytical Methods in Fine Particle Technology," Micromeritics Instrument Co., Norcross, GA USA, 17 (1997).